Fault-controlled hydration of the upper mantle during continental rifting

Bayracki, Gaye; Minshull, Tim; Sawyer, Dale; Reston, Timothy; Klaeschen, Dirk; Papenberg, Cord; Ranero, Cesar; Bull, Jonathan; Davy, Richard; Shillington, Donna; Perez Gussinye, Marta; Morgan, Julia

DOI:
10.1038/ngeo2671

Document Version
Peer reviewed version

Citation for published version (Harvard):
Bayracki, G, Minshull, T, Sawyer, D, Reston, T, Klaeschen, D, Papenberg, C, Ranero, C, Bull, J, Davy, R, Shillington, D, Perez Gussinye, M & Morgan, J 2016, 'Fault-controlled hydration of the upper mantle during continental rifting', *Nature Geoscience*, vol. 9, pp. 384-388. https://doi.org/10.1038/ngeo2671

Fault-controlled hydration of the upper mantle during continental rifting

G. Bayrakci[1], T. A. Minshull[1*], D. S. Sawyer[2], T. J. Reston[3], D. Klaeschen[4], C. Papenberg[4], C. Ranero[5], J. M. Bull[1], R. G. Davy[1], D. J. Shillington[6], M. Perez-Gussinye[7], J. K. Morgan[2]

1- University of Southampton, Ocean and Earth Science, National Oceanography Centre Southampton, Southampton, United Kingdom

2- Rice University, Department of Earth Science, Houston, United States

3- University of Birmingham, School of Geography, Earth and Environmental Sciences, Birmingham, United Kingdom

4- GEOMAR, Helmholtz Centre for Ocean Research Kiel, Marine Geodynamics, Kiel, Germany

5- ICREA at CSIC, Barcelona Centre for Subsurface Imaging, Instituto de Ciencias del Mar, Barcelona, Spain

6- Lamont-Doherty Earth Observatory of Columbia University, Marine Geophysics, Palisades, United States

7- Royal Holloway University of London, Department of Earth Sciences, London, United Kingdom

Water and carbon are transferred from the ocean to the mantle in a process that alters mantle peridotite to create serpentinite and supports diverse ecosystems[1]. Serpentinised mantle rocks are found beneath the seafloor at slow- to ultraslow-spreading mid-ocean ridges[1] and are thought to be present at about half the world's rifted margins[2,3]. Serpentinite is also inferred to exist in the downgoing

plate at subduction zones[4], where it may trigger arc magmatism or hydrate the deep Earth. Water is thought to reach the mantle via active faults[3,4]. Here we show that serpentinisation at the rifted continental margin offshore from western Spain was probably initiated when the whole crust cooled to become brittle and deformation was focused along large normal faults. We use seismic tomography to image the three-dimensional distribution of serpentinisation in the mantle and find that the local volume of serpentinite beneath thinned, brittle crust is related to the amount of displacement along each fault. This implies that seawater reaches the mantle only when the faults are active. We estimate the fluid flux along the faults and find it is comparable to that inferred for mid-ocean ridge hydrothermal systems. We conclude that brittle processes in the crust may ultimately control the global flux of seawater into the Earth.

The formation of serpentinite requires a supply of fluids to the mantle, but the bulk continental crust typically has low permeabilities (10^{-14} to 10^{-18} m^2)[(5)]. Active faults have been shown to transmit fluids during earthquakes and fault damage zones form potential fluid pathways[6], but low-permeability fault gouge can be a barrier to fluid flow[7]. In short, the complex distribution of low and high permeability features within fault zones leads to extreme permeability heterogeneity and anisotropy[7], so that the importance of faults as fluid pathways over geological timescales is unclear.

During rifting at magma-poor continental margins, crustal thinning leads to a reduction in overburden pressure at depth, which together with cooling moves the originally viscous lower crust into the brittle field[3]. Numerical models that track the thermal and rheological evolution of rifted margins have suggested that, for a wide range of strain rates and starting rheologies, the entire crust should become brittle at thicknesses of

between 14 and 4 km (Fig. 1a). Sufficient coincident deep seismic reflection and refraction profiles across magma-poor rifted margins now exist to enable a rigorous comparison between the observed maximum crustal thickness above or juxtaposed against serpentinised mantle, and the thickness at which complete crustal embrittlement is expected to occur[8] (Fig. 1 and Supplementary Fig. S1; Methods). Our compilation shows that serpentinite is found only where the crust is thin enough to have become entirely brittle during rifting and for many margins, such as Porcupine Basin[9] and Southeast Flemish Cap[10], conjugate to Galicia margin the predictions exactly match the observations (Fig. 1a-c and Supplementary Fig. S1). At some margins (e.g., Nova Scotia[11]; Fig. 1e and Supplementary Fig. S1) serpentintite only occurs beneath crust both thinner and some distance oceanward than predicted. However, in each case thick synrift sediments and/or salt, both known to reduce permeability[12], are present. It is clear that a brittle crust is not the only criterion for the serpentinisation; suitable fluid pathways must also exist. Perhaps most intriguingly, at other margins, the misfit is small, with serpentinite only occurring under crust that is thinner than predicted but only about a fault block spacing (5-10 km) further oceanward than predicted (Figs. 1a and d, Supplementary Fig. S1). This observation suggests that the serpentinisation process may be controlled by faults cutting down from the seafloor to the mantle. Thus at all serpentinite margins, where block bounding normal faults are well imaged, there is a strong link between the presence and the spacing of the brittle faulting in the thin crust and the serpentinisation of the underlying mantle.

The Deep Galicia segment of the magma-poor west Iberia rifted margin (Figs 1 and 2d) is one such margin. Here, rifting led to the formation of hyperextended continental crust with serpentinisation, detachment faulting and subsequent mantle exhumation[13]. Serpentinite has a lower density and coefficient of friction than fresh mantle peridotite

and causes weakening of the mantle[14]. The most recent normal faults soled out into the weaker serpentinite layer, forming a detachment-like surface at the boundary between the fault-bounded tilted crustal blocks and serpentinised mantle, a boundary described from seismic reflection profiles as the "S reflector"[13].

We compare the 3D compressional (P-) wave velocity structure of the Deep Galicia Margin obtained from first-arrival travel-time tomography (Methods) with tectonic structure from representative pre-stack depth migrated multi-channel seismic reflection profiles, migrated using independent velocity models (Fig. 2). We obtained velocities similar to those previously obtained from a two-dimensional transect through the same area[15], but our denser sampling and 3D survey geometry (Supplementary Figs. S2 and S3) yield much improved resolution. The smooth velocity model closely matches the 5-10 km wide tilted basement blocks imaged on the seismic profiles. From the interpreted top of the crystalline basement down to the S reflector, velocities vary between 5.5 and 6.5 km/s; the 6.5 km/s iso-velocity contour follows closely the S reflector where it underlies the tilted basement blocks (root-mean-square difference 0.4 km), illustrating the resolution of the model, confirmed using standard resolution tests (Supplementary Information, Supplementary Figs. S4 - S7) for velocities both above and below S. Velocities beneath the S reflector increase to 7.5 km/s over a mean depth interval of 1.2 km. If these velocity variations are attributed solely to variations in the degree of serpentinisation, they would correspond to a decrease from ~45% serpentinisation (6% by weight of water) immediately below the S reflector to ~15% at depths of ~1.2 km below the S reflector. The inversion yields a smooth, isotropic model. Anisotropy is likely to be present in the uppermost mantle but limited to a few per cent when velocities are reduced by serpentinisation to 6.5-7.5 km/s[16].

Intriguingly, at the intersections between the block-bounding normal faults and the S reflector, this velocity increase occurs over a larger depth interval (~2 km), suggesting a locally thicker zone of highly serpentinised mantle (Figs. 2 and 3a). This observation implies that faults in the hanging-wall of the S reflector have had a role in the transport of seawater to the mantle. Alternatively, velocities could be reduced by the presence beneath S of lower crustal material or of frozen melt. However, lower crustal material is unlikely because none is imaged on coincident seismic reflection profiles, and mafic intrusions are also unlikely as no magmatism is known at this margin, and we would not expect its location to be controlled by faulting processes above S.

The volume of seawater supplied to the mantle has been estimated from the volume of the serpentinised region and the degree of serpentinisation (Methods). Each block-bounding fault is associated with a maximum in water uptake, implying not only that the water uptake was controlled by the deformation associated with those faults but also that the serpentinised mantle has subsequently moved with the overlying fault blocks, requiring the S detachment progressively to have become inactive, as expected for brittle sequential faulting[17] such as in rolling hinge model[18]. Hydrothermal systems commonly involve focused upflow along faults and diffuse downflow away from faults[19]. Our data only tell us the water volume required for the observed degree of serpentinisation, from which we infer the total net downflow during serpentinisation (Methods). The inferred net downflow (minimum time-integrated flux) for individual faults varies between 1.2×10^4 and 5.9×10^4 m^3 per square metre of fault cross-sectional area. There are very few published estimates for comparison, but our estimated time integrated fluxes are comparable to values of $\sim 10^5$ m^3/m^2 inferred for mid-ocean ridge faults in the Oman Ophiolite[20].

Along the southernmost profile the fault that intersects the S reflector beneath the basin oceanward of the last continental fault block (Supplementary Fig. S8c, F6, profile ISE1), is not used for the estimation of time integrated fluxes. At that location the observed high degree of serpentinisation may be due to the direct connection at breakup time between the ocean and the exhumed foot-wall mantle. This environment may have been similar to off-axis, low-temperature, ultra-mafic hosted foot-wall hydrothermal systems observed at mid-ocean ridges[21].

The strong correlation between the water volumes and the fault displacements (correlation coefficient: 0.91, probability of no correlation: 0.006; Fig. 3c and Supplementary Figs. S9 - S10; Methods) suggests that a physical process links these parameters, perhaps associated with increased connectivity of fluid pathways when faults move[22]. If we assume that the faults above the S reflector moved sequentially to accommodate a constant extension rate[17], the duration of their activity, and therefore the corresponding flow rates, may be inferred from their displacement (Methods). Inferred flow rates vary between 6.2×10^{-8} and 3.8×10^{-7} $m^3 s^{-1}$ per metre along the rift. These rates are around one order of magnitude less than those associated with high-temperature fluid fluxes at the TAG hydrothermal field, where a flux of ~100 kg/s[(23)] is inferred to be sourced from 35-61 km of rift[24], corresponding to a flow rate of $2\text{-}3 \times 10^{-6}$ $m^3 s^{-1}$ per metre.

Water circulation in the crust may be driven by episodic changes in tectonic stress and in fault zone permeability[6]. A combination of coupled fluid pressure and mean stress, suction pumping action and fault-valve action leads to the cyclic accumulation of water, followed by fault reactivation and release of fluids[25]. Rather than using the fault damage zone, the downflow may occur through antithetic faults created at the tips of

normal faults when they penetrate into regions of reduced yield stress[6], with any upflow through the fault damage zone. At the Deep Galicia Margin such antithetic faults might have started to form where the normal faults sole out onto the S reflector detachment surface. As the opening of such antithetic faults is driven by the slip cycle on the main block-bounding fault, fluid flow will also be proportional to the slip on that fault, explaining the fit in Figure 3c. This latter mechanism may explain why serpentinisation appears to be focused beneath the hanging-walls of the normal faults detaching onto S (Fig. 2).

We do not infer 100% serpentinisation anywhere below the S reflector. The production of new serpentinite depends on the temperature of the medium and the access of the water to the unreacted peridotite, which is controlled by the water supply and the porosity and the permeability of the medium[26,27]. Serpentinite has a lower permeability (10^{-23} -10^{-22} m^2) than crustal rocks and faults and serpentinisation is a volume-increasing process (up to 40% of volume expansion[3,27]) that reduces the initial rock porosity to near zero. However, due to the volume expansion, cracking occurs and locally increases the permeability. Within the serpentinite the water flow uses these cracks and is driven by the pressure gradient created by the serpentinisation[27]. The incomplete serpentinisation may suggest an insufficient water supply, in which case all of the available water may have been consumed.

Alternatively, high temperatures and/or the limited access of the water to fresh mantle peridotite may have resulted in a low serpentinisation rate. In that case, the water may have been recycled by upflow along the faults. At the onset of serpentinisation during continental breakup, the crust is less than 14 km thick (Fig. 1a), and the mantle is at around 400-500 °C, i.e. the upper limit of the serpentinite stability[26]. The geothermal

gradient is high and remains high due to heat released during serpentinisation, providing suitable conditions for focused upflow along the fault damage zones. If such hydrothermal circulation is initiated, it will continue until the pore-filling reactions between the hydrothermal fluids and the cold crustal rocks and ambient fluids lower the damage zone permeability again[22].

Here we quantified the fluid fluxes in a rifted margin setting, but our approach could also be at mid-ocean ridges and subduction zones given seismic data of sufficient resolution. Our results show that when the entire crust becomes brittle during extension, bulk serpentinisation in the upper 2 km of the mantle is enhanced close to crustal faults, and thus that hydration of the upper mantle is fault-controlled. Therefore brittle processes in the crust ultimately may control the global flux of seawater into the solid Earth.

197 **References**

198

199 1. Fruh-Green, G.L., et al., *Serpentinization of oceanic peridotites: Implications for*
200 *geochemical cycles and biological activity.* Subseafloor Biosphere at Mid-Ocean
201 Ranges, 2004. **144**: p. 119-136.

202 2. Whitmarsh, R.B., et al., *Tectonic implications of exposure of lower continental crust*
203 *beneath the Iberia Abyssal Plain, Northeast Atlantic Ocean: Geophysical evidence.*
204 Tectonics, 2000. **19**(5): p. 919-942.

205 3. Perez-Gussinye, M. and T.J. Reston, *Rheological evolution during extension at*
206 *nonvolcanic rifted margins: Onset of serpentinization and development of detachments*
207 *leading to continental breakup.* Journal of Geophysical Research-Solid Earth, 2001.
208 **106**(B3): p. 3961-3975.

209 4. Ranero, C.R., et al., *Bending-related faulting and mantle serpentinization at the Middle*
210 *America trench.* Nature, 2003. **425**(6956): p. 367-373.

211 5. Manning, C.E. and S.E. Ingebritsen, *Permeability of the continental crust: Implications*
212 *of geothermal data and metamorphic systems.* Reviews of Geophysics, 1999. **37**(1): p.
213 127-150.

214 6. Sibson, R.H., *Fluid involvement in normal faulting.* Journal of Geodynamics, 2000.
215 **29**(3-5): p. 469-499.

216 7. Faulkner, D.R., et al., *A review of recent developments concerning the structure,*
217 *mechanics and fluid flow properties of fault zones.* Journal of Structural Geology, 2010.
218 **32**(11): p. 1557-1575.

219 8. Reston, T.J., *The structure, evolution and symmetry of the magma-poor rifted margins*
220 *of the North and Central Atlantic: A synthesis.* Tectonophysics, 2009. **468**(1–4): p. 6-27.

221 9. O'reilly, B.M., et al., *Crustal thinning, mantle exhumation and serpentinization in the*
222 *Porcupine Basin, offshore Ireland: evidence from wide-angle seismic data.* Journal of

the Geological Society, 2006. **163**: p. 775-787.

10. Funck, T., et al., *Crustal structure of the ocean-continent transition at Flemish Cap: Seismic refraction results.* Journal of Geophysical Research-Solid Earth, 2003. **108**(B11).

11. Zelt, C.A., et al., *Assessment of crustal velocity models using seismic refraction and reflection tomography (vol 153, pg 609, 2003).* Geophysical Journal International, 2003. **154**(1): p. 230-230.

12. Wu, Y., et al., *Crustal structure of the central Nova Scotia margin off Eastern Canada.* Geophysical Journal International, 2006. **166**(2): p. 878-906.

13. Rupke, L.H., et al., *Interrelation between rifting, faulting, sedimentation, and mantle serpentinization during continental margin formation-including examples from the Norwegian.* Geochemistry Geophysics Geosystems, 2013. **14**(10): p. 4351-4369.

14. Reston, T.J., et al., *Movement along a low-angle normal fault: The S reflector west of Spain.* Geochemistry Geophysics Geosystems, 2007. **8**.

15. Escartin, J., G. Hirth, and B. Evans, *Effects of serpentinization on the lithospheric strength and the style of normal faulting at slow-spreading ridges.* Earth and Planetary Science Letters, 1997. **151**(3-4): p. 181-189.

16. Ranero, C.R. and M. Perez-Gussinye, *Sequential faulting explains the asymmetry and extension discrepancy of conjugate margins.* Nature, 2010. **468**(7321): p. 294-U180.

17. Borgmeyer, A.L., *Three-dimensional geometries of rifting on a hyperextended margin - Interpretation of seismic reflection profiles from the Deep Galicia Basin, Iberia*. 2010, Rice University.

18. Christensen, N.I., *Serpentinites, peridotites, and seismology.* International Geology Review, 2004. **46**(9): p. 795-816.

19. Buck, W.R., *Flexural rotation of normal faults.* Tectonics, 1988. **7**(5): p. 959-973.

20. Kelley, D.S., J.A. Baross, and J.R. Delaney, *Volcanoes, fluids, and life at mid-ocean*

ridge spreading centers. Annual Review of Earth and Planetary Sciences, (2002) **30(1), 385-491**.

21. Coogan, L.A., et al., *Chemical and thermal constraints on focussed fluid flow in the lower oceanic crust.* American Journal of Science, 2006. **306**(6): p. 389-427.

22. Fruh-Green, G.L., et al., *30,000 years of hydrothermal activity at the Lost City vent field.* Science, 2003. **301**(5632): p. 495-498.

23. Reynolds, S.J. and G.S. Lister, *Structural Aspects of Fluid-Rock Interactions in Detachment Zones.* Geology, 1987. **15**(4): p. 362-366.

24. Hannington, M.D., et al, *Comparison of the TAG mound and stockwork complex with Cyprus-trype massive sulphide deposit.* . Proceedings of the Ocean Drilling Program, Scientific Results, 1998. **158**: p. 389-415.

25. Baker, E.T., *Hydrothermal cooling of midocean ridge axes: Do measured and modeled heat fluxes agree?, Earth and Planetary Science Letters.* 2007 **263,**(1–2): p. 40-150.

26. Sibson, R.H., *Generation of Pseudotachylyte by Ancient Seismic Faulting.* Geophysical Journal of the Royal Astronomical Society, 1975. **43**(3): p. 775-&.

27. Emmanuel, S. and B. Berkowitz, *Suppression and stimulation of seafloor hydrothermal convection by exothermic mineral hydration.* Earth and Planetary Science Letters, 2006. **243**(3-4): p. 657-668.

28. Macdonald, A.H. and W.S. Fyfe, *Rate of Serpentinization in Seafloor Environments.* Tectonophysics, 1985. **116**(1-2): p. 123-135.

Acknowledgements

We thank all who sailed with us on *R/V Marcus Langseth* and *F/S Poseidon* for their hard work at sea, Marianne Karplus for assistance with detailed survey design and Anne Krabbenhoft for assistance with data processing. This research was supported by the US National Science Foundation, the UK Natural Environment Research Council (NE/E016502/1) and GEOMAR Helmholz Centre for Ocean Research. Ocean bottom instruments were provided by the UK Ocean Bottom Instrumentation Facility and by GEOMAR. T.A.M. was supported by a Wolfson Research Merit award.

Author Contributions

D.S.S., T.J.R., T.A.M., D.K., D.J.S., C.R., J.B. and J.K.M. designed the seismic experiment. D.S.S. led the survey on *R/V Marcus Langseth* and D.K. and C.P. led the deployment and recovery of seafloor instruments aboard *F/S Poseidon*. G.B. conducted the seismic data analysis, with some assistance from R.G.D. T. J. R. compiled the North Atlantic seismic profiles and M.P.G. carried out the numerical modelling. G.B. and T.A.M. wrote the first draft of the paper and all authors contributed to subsequent revisions.

Additional Information

Supplementary information is available in the online version of the paper. Reprints and permissions information is available online at www.nature .com/reprints. Correspondence and requests for materials should be addressed to T.A.M

Competing financial interests

The authors have no competing financial interests.

297 **Figure Legends**

298 **Figure 1: a)** Comparison between the crustal thickness at which complete crustal
299 embrittlement is predicted to occur[3] (grey region covering three different modelled
300 rheologies) and the maximum crustal thickness observed above or juxtaposed against
301 serpentinised mantle at various North Atlantic magma-poor margins[8]. NS: Nova Scotia,
302 PB: Porcupine Basin, FC: Flemish Cap, IAP: Iberian Abyssal Plain, ARM: Armorican
303 Margin, NB: Newfoundland Basin, TAP: Tagus Abyssal Plain. The prefixes W, E, N, S
304 are West, East, North and South respectively. Cross sections of **b)** Porcupine Basin[9], **c)**
305 Southeast Flemish Cap[10], **d)** Galicia[15] and **e)** Nova Scotia[11] margins.

306

307 **Figure 2:** Compressional (P-) wave velocities superimposed on coincident seismic
308 reflection profiles illustrate the concentration of serpentinisation beneath the hanging-
309 wall of normal faults (expansion of 6.5 – 7.5 km/s iso-velocity interval). Yellow circles
310 are seabed instrument locations. Iso-velocity contours are marked by thin black lines.
311 Dashed lines mark the seabed (pale blue), interpreted base of post-rift sediments (green),
312 top of the pre-rift sediments (blue), top of the crystalline basement (red), S reflector
313 (black). Thick black lines indicate faults. **a)** ISE4 profile[13]; **b)** IAM 11 profile[17]; **c)** ISE1
314 profile[28]; **d)** location of the Galicia 3D survey with colour-coded bathymetry. **e)**
315 Schematic illustrating serpentinization associated with a single normal fault "F".

316

317 **Figure 3:** Water volume and amount of serpentinisation associated with faults on the
318 seismic reflection profile shown in Fig. 2b, assuming a two-dimensional structure. **a)**
319 Degree of serpentinisation (white contours) and water content (black contours). Black
320 and green boxes show the vertical and horizontal integration domains, respectively.
321 Bold black lines are the faults and dashed black line is the S reflector. **b)** Vertically
322 integrated water content (black) and horizontal extent associated with faults (green). **c)**

Correlation between water volume within hydrated mantle, representing integrated net fluid flux through the fault, and fault displacement at the top of crystalline basement. Data derived from seismic profiles (Fig. 2a – c) are shown by the magenta, green and blue colors respectively. Faults F4 – F6 are shown by the triangle, square and circle symbols respectively.

Methods

We calculated the stretching factor at which the entire crust becomes brittle using hundreds of runs of a one-dimensional numerical model, in which a 125-km lithosphere with a 32 km crust undergoes extension by a uniform pure strain rate[3]. The initial basal and Moho temperatures were 1300^{o} of 550^{o} C, respectively[3]. We used a wet quartz rheology for the upper crust, anorthosite, dry quartz and aggregate rheologies for the lower crust, and a dry olivine rheology for the mantle[3]. For various Atlantic rifted margins, we used published profiles showing the depth to the top of crystalline crust from seismic reflection data and the depth to the Moho and distribution of mantle serpentinisation from wide-angle seismic data (Supplementary Fig. S1). From these profiles, we determined the maximum crustal thickness either beneath which detectable serpentinisation occurs (e.g. Galicia), or where crust and serpentinite are juxtaposed (e.g. S Iberia Abyssal Plain).

Seismic data on the Deep Galicia Margin were collected between June and September 2013. The primary aim of the survey was to acquire a three-dimensional seismic reflection volume. Airgun shots were fired from *R/V Marcus Langseth* along fifty parallel profiles with 400 m spacing between them (Supplementary Fig. S2), alternating between two 3000 cu. in. airgun arrays to give a shot interval of 37.5 m (~16 s). A grid of 72 ocean bottom instruments, comprising 44 four-component ocean bottom seismometers (OBSs) and 28 ocean bottom hydrophones (OBHs) was deployed on the seabed for three months to record these shots, with sample rates of 250 Hz and 200 Hz, respectively. OBS/H data were corrected for internal clock drifts and instruments were relocated using a 2D iterative inversion (Supplementary Information). In our analysis we used first arrival travel-times from 48 OBS/H spread across the survey area (Supplementary Fig. S2). The pick uncertainty was estimated visually as a function of

signal noise ratio and varied from 50 to 230 ms.

The P-wave velocity image was constructed using a non-linear iterative tomographic technique (FAST[29]). A total of 155,924 first arrival times was used, corresponding mostly to crustal refractions, since there are few first arrivals from shallower parts of the structure (Supplementary Fig. S3). We used a forward grid of 0.5 km node interval and an inverse grid of 1 km cell size. The starting models used in this study and the resolution and uncertainty of the inversion results are discussed in the Supplementary Information (Supplementary Figs. S4 – S7).

P-wave velocities were converted to percentage of serpentinization below the depth of the S reflector and the water content by weight was estimated using an empirical relationship[30] (Fig. 3 and Supplementary Fig. S8). The water content may be overestimated because of model smoothing across a velocity discontinuity. The weight of serpentinite was calculated using the estimated density of the serpentinite at each grid node and the water weight percentages were used to calculate the water volume. The water volume associated with a given block-bounding normal fault was estimated by integrating the water volume over a vertical interval of 2.5 km beneath the S reflector and a horizontal interval of 7 km (Fig. 3 and Supplementary Fig. S8). The bottom of the depth interval was chosen to be close to the limit of ray coverage (Supplementary Fig. S5). The horizontal integration interval approximates the width of the region of reduced velocities around an isolated fault (Figs 2b and 3a, F5, profile IAM 11). The values resulting from the vertical and horizontal integration (Fig. 3c) represent the water volume per unit length along the margin that is associated with a given fault. Some of this fluid will have been fed by the S detachment itself, perhaps represented by the intercept on the vertical axis of the regression line shown in Fig. 3c. The minimum time-

integrated fluxes are estimated by dividing the water content associated with the faults by the thickness of the faults. A thickness of 50 m was inferred for the S reflector by the full waveform inversion along profile ISE1[31], and for this approximate calculation we assume that the block-bounding faults have comparable thickness.

Fault displacements at the top of crystalline basement were estimated from foot-wall and hanging-wall cut-off[32] measured for each fault block, on pre-stack depth migrated seismic profiles (Fig. 2a-c and Supplementary Fig. S9). Due to the topography of the crystalline basement, a minimum and a maximum displacement were calculated for each fault and the mean displacement was used in the discussion. Water content estimation errors were calculated using the standard deviations of the P-wave velocity at the nodes (Fig. 3c and Supplementary Fig. S7). We estimated the duration of activity of the faults by dividing the heaves by the half extension rate of 0.8±0.36 cm/yr[33]. We then estimated the flow rates by dividing the water volume related with one fault by the duration of activity of that fault.

Code Availability: The tomographic FAST[29] code used for this study is available at http://terra.rice.edu/department/faculty/zelt/fast.html

29. Zelt, C.A. and P.J. Barton, *Three-dimensional seismic refraction tomography: A comparison of two methods applied to data from the Faeroe Basin.* Journal of Geophysical Research-Solid Earth, 1998. **103**(B4): p. 7187-7210.
30. Carlson, R.L. and D.J. Miller, *Mantle wedge water contents estimated from seismic velocities in partially serpentinized peridotites.* Geophysical Research Letters, 2003. **30**(5).
31. Leythaeuser, T., T.J. Reston, and T.A. Minshull, *Waveform inversion of the S reflector west of Spain: Fine structure of a detachment fault.* Geophysical Research Letters, 2005. **32**(22).
32. Mansfield, C. and J. Cartwright, *Fault growth by linkage: observations and implications from analogue models.* Journal of Structural Geology, 2001. **23**(5): p. 745-763.
33. Sutra, E., et al., *Quantification and restoration of extensional deformation along the Western Iberia and Newfoundland rifted margins.* Geochemistry Geophysics Geosystems, 2013. **14**(8): p. 2575-2597.

Figures

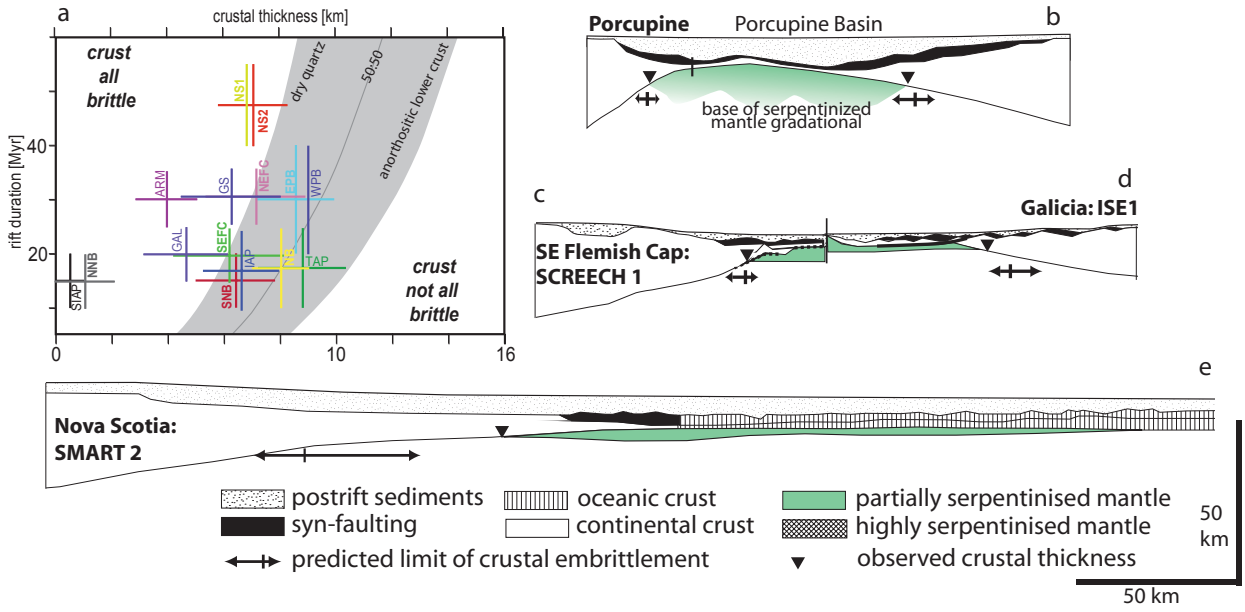

Figure 1: Comparison between the crustal thickness at which complete crustal embrittlement is predicted to occur[3] and the maximum crustal thickness observed above or juxtaposed against serpentinised mantle at various a) Modelling results showing the crustal thickness at which the entire crust becomes brittle (grey region covering three different modelled rheologies).North Atlantic magma-poor margins[8]. NS: Nova Scotia, PB: Porcupine Basin, FC: Flemish Cap, IAP: Iberian Abyssal Plain, GS: Goban Spur, ARM: Armorican Margin, GAL: Galicia, NB: Newfoundland Basin, TAP: Tagus Abyssal Plain. The prefixes W, E, N, S are West, East, North and South respectively. Cross sections of **b)** Porcupine Basin[9], **c)** Southeast Flemish Cap[10], profile SCREECH-1, **d)** Galicia[11], profile ISE-1, and **e)** Nova Scotia[12], profile SMART-2.

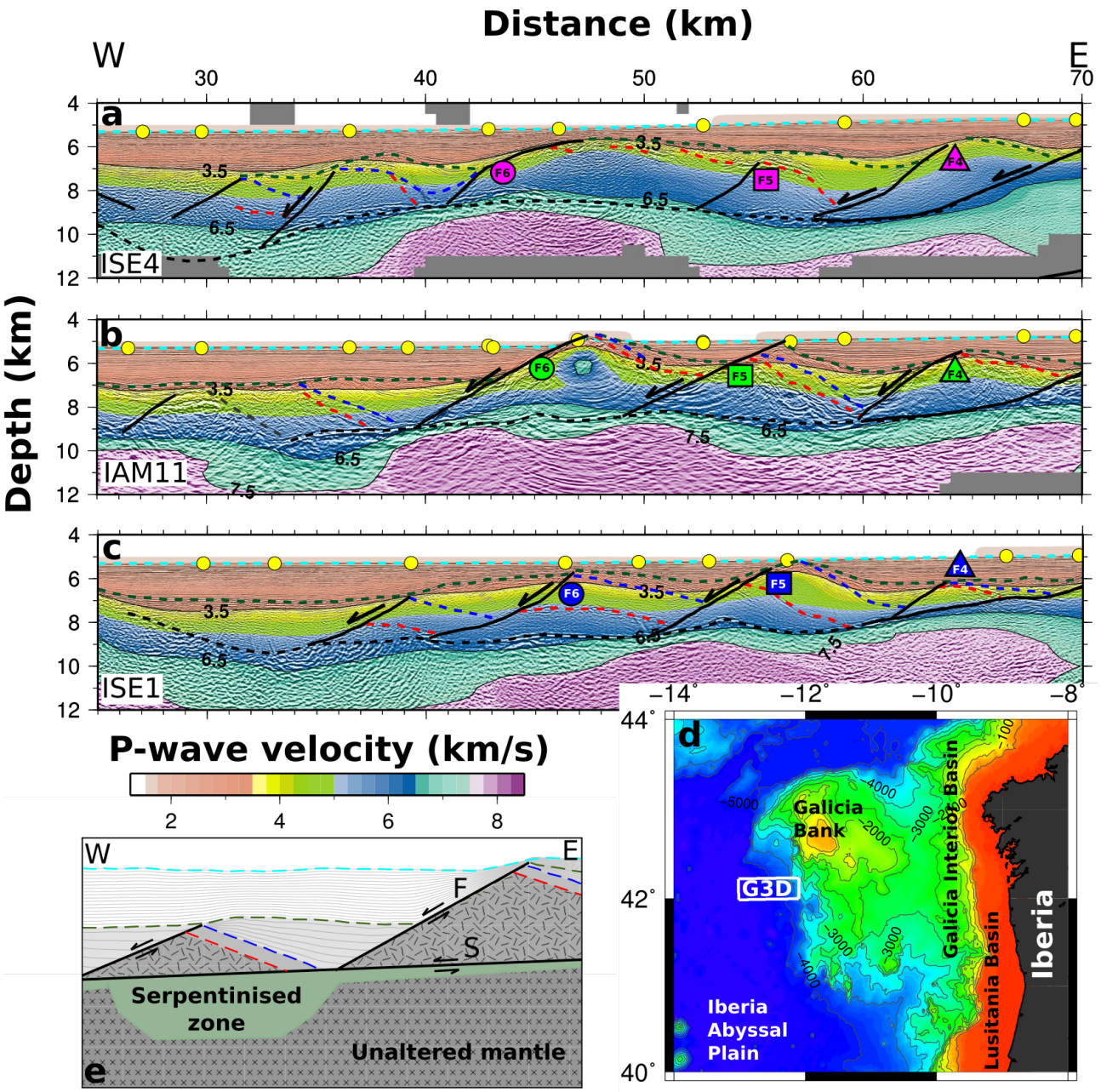

Figure 2: Compressional (P-) wave velocities superimposed on coincident seismic reflection profiles illustrate the concentration of serpentinisation beneath the hanging-wall of normal faults (expansion of 6.5 – 7.5 km/s iso-velocity interval). Yellow circles are seabed instrument locations. Iso-velocity contours are marked by thin black lines. Dashed lines mark the seabed (pale blue), interpreted base of post-rift sediments (green), top of the pre-rift sediments (blue), top of the crystalline basement (red), S reflector (black). Thick black lines indicate faults. **a)** ISE4 profile[14]; **b)** IAM 11 profile[16]; **c)** ISE1 profile[17]; **d)** location of the Galicia 3D survey with colour-coded bathymetry. **e)** Schematic illustrating serpentinization associated with a single normal fault "F".

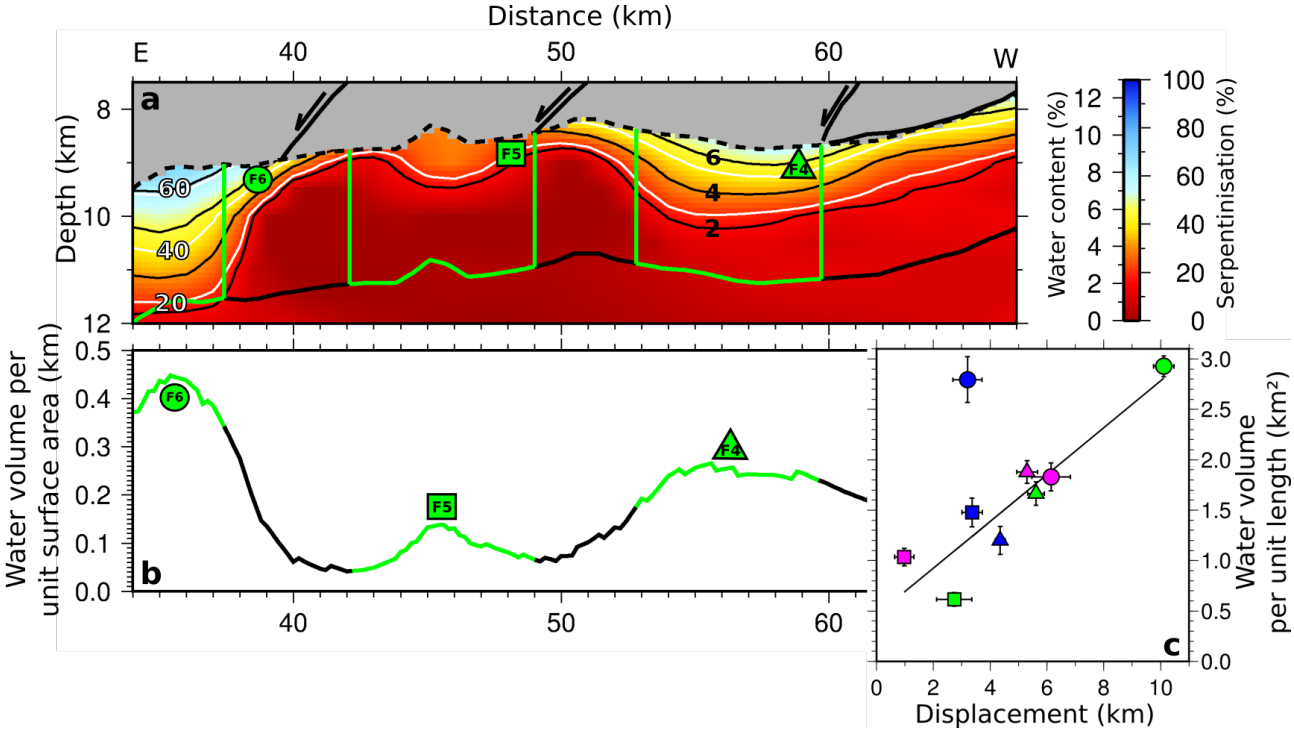

Figure 3: Water volume and amount of serpentinisation associated with faults on the seismic reflection profile shown in Fig. 2b, assuming a two-dimensional structure. **a)** Degree of serpentinisation (white contours) and water content (black contours). Black and green boxes show the vertical and horizontal integration domains, respectively. Bold black lines are the faults and dashed black line is the S reflector. **b)** Vertically integrated water content (black) and horizontal extent associated with faults (green). **c)** Correlation between water volume within hydrated mantle, representing integrated net fluid flux through the fault, and fault displacement at the top of crystalline basement. Data derived from seismic profiles (Fig. 2a – c) are shown by the magenta, green and blue colors respectively. Faults F4 – F6 are shown by the triangle, square and circle symbols respectively.